Journal of ELECTRONIC MATERIALS, Vol. 41, No. 8, 2012
DOI: 10.1007/s11664-012-2079-5
© 2012 TMS

Modeling Fracture of Sn-Rich (Pb-Free) Solder Joints Under Mechanical Shock Conditions

HUIYANG FEI,[1] KYLE YAZZIE,[2] NIKHILESH CHAWLA,[1,2] and HANQING JIANG[1,3]

1.—Mechanical and Aerospace Engineering, School for Engineering of Matter, Transport and Energy, Fulton Schools of Engineering, Arizona State University, Tempe, AZ 85287-8706, USA. 2.—Materials Science and Engineering, School for Engineering of Matter, Transport and Energy, Fulton Schools of Engineering, Arizona State University, Tempe, AZ 85287-8706, USA. 3.—e-mail: hanqing.jiang@asu.edu

With the increasing focus on developing environmentally benign electronic packages, lead-free solder alloys have received a great deal of attention. Mishandling of packages during manufacture, assembly, or by the user may cause solder joint failure. In this work, we conducted finite-element analysis to model solder joint fracture under dynamic loading conditions. The solder is modeled as a porous plastic material, and the intermetallic compound (IMC) material is characterized as an elastic material. The fracture of the solder is governed by void nucleation, and the IMC fracture is brittle in nature. The randomness of the void volume fraction in the solder and the defects in the IMC are considered and implemented in the finite-element package ABAQUS. The finite-element results show that the fracture mechanisms of the solder joints depend on the strain rate and IMC thickness. High strain rate and larger IMC thickness favor IMC-controlled fracture, which is brittle in nature. Low strain rate and smaller IMC thickness lead to solder-controlled fracture, which is governed by void growth and nucleation. Based on this finding, a mechanistic explanation for solder joint fracture is suggested.

Key words: Lead-free solder joint, porous plasticity, brittle fracture, strain rate

INTRODUCTION

Because of the environmental concerns over lead (Pb)-containing solders, Pb-free solders, such as Sn-Ag-Cu and Sn-Ag alloys, have been widely used in electronic packaging. Solder joints must retain their mechanical integrity under a variety of mechanical loads in service, including creep, thermal fatigue, and mechanical shock.[1–8] The mechanical performance and reliability of solder joints are controlled by the behavior of the Sn-rich alloy and the intermetallic compound (IMC) formed between Sn and the metallization. In the case of copper metallization, the IMC of interest is Cu_6Cn_5.

Very few systematic studies on the mechanical shock behavior of solders exist. Chawla[9] hypothesized that solder joint fracture is controlled by the solder at relatively low strain rates and moves toward IMC-controlled fracture at high strain rates. This is because, at lower strain rates, the solder is able to relax stress by plastic deformation, while at higher strain rates, the stress state is more triaxial. In many reports, fracture at or within the IMC layer is observed.[10–12] Suh et al.[10] showed that, by decreasing the content of Sn in a Sn-Ag-Cu (SAC) solder material, the fracture mode shifts from IMC failure in the higher-Ag-content material to that of failure within the solder at lower Ag content. Liu et al.[11] found that solder aging decreased the drop resistance of the solder joint, although it is not clear whether this is due to an increase in IMC thickness or a decrease in solder strength. Mattila et al.[12]

(Received August 31, 2011; accepted March 20, 2012; published online April 10, 2012)

studied the mechanical drop behavior of several solder and metallization combinations. They hypothesized that the main failure mechanism under mechanical shock loading is related to the high deformation rates and strain-rate hardening of the solder, which forces cracks to propagate in the IMC layers instead of the bulk solder. Fei et al.[13] studied void-induced solder-based fracture using a porous plasticity model, namely the Gurson–Tvergaard–Needleman (GTN) model, considering the randomness of the initial voids in the analysis. By considering the initial random voids, various crack paths can be captured while the macroscopic behavior remains unchanged. A systematic modeling effort to show the transition from solder-controlled to IMC-controlled fracture is required.

In this work, we conducted finite-element analysis to study the fracture behavior of single solder joints by coupling void-induced solder-based fracture and IMC-controlled brittle fracture. To capture the effect of defects in the IMC, we model the IMC as an inhomogeneous material with material properties varying with location. Because of the complexity of solder joint behavior, the present paper attempts to establish a methodology that enables qualitative understanding of some observed experimental phenomena.

The structure of the paper is the following. "Finite-Element Modeling Approach" section reviews the porous plastic model used in the solder material with a random initial distribution of voids[13] and introduces the details of the finite-element model used to study the fracture mechanism of the solder joints. The effects of inhomogeneity, thickness, and shape of the IMC as well as the applied strain rate on the solder joint are described and discussed in "Results and Discussion" section. "Conclusions" section provides a theoretical and qualitative pictorial explanation of solder joint failure.

FINITE-ELEMENT MODELING APPROACH

In Pb-free solder alloys, particularly Sn-rich solders with Ag and Cu, second-phase particles, such as Ag_3Sn and Cu_6Sn_5, are present in the Sn matrix. Thus, microscopic voids are nucleated at these second-phase particles, as observed by fractographic analysis.[14,15] An example of such a fracture surface is shown in Fig. 1. It should be pointed out that fracture mainly occurs as a result of voids instead of grain boundaries, particularly under mechanical shock conditions.

Porous plasticity models, such as that of GTN, also called the modified Gurson model, have been widely used in modeling microvoid-induced ductile fracture. In the GTN model the void volume fraction, f, is defined as the volume of voids divided by the total volume of porous material ($f = 0$ describes a fully dense material and $f = 1$ represents a fully voided material). The GTN model proposes a yield surface given by[16,17]

$$\phi = \left(\frac{\sigma_e}{\sigma_y}\right)^2 + 2q_1 f \cosh\left(-\frac{3q_2}{2\sigma_y}\sigma_{kk}\right) - (1 + q_3 f^2) = 0, \quad (1)$$

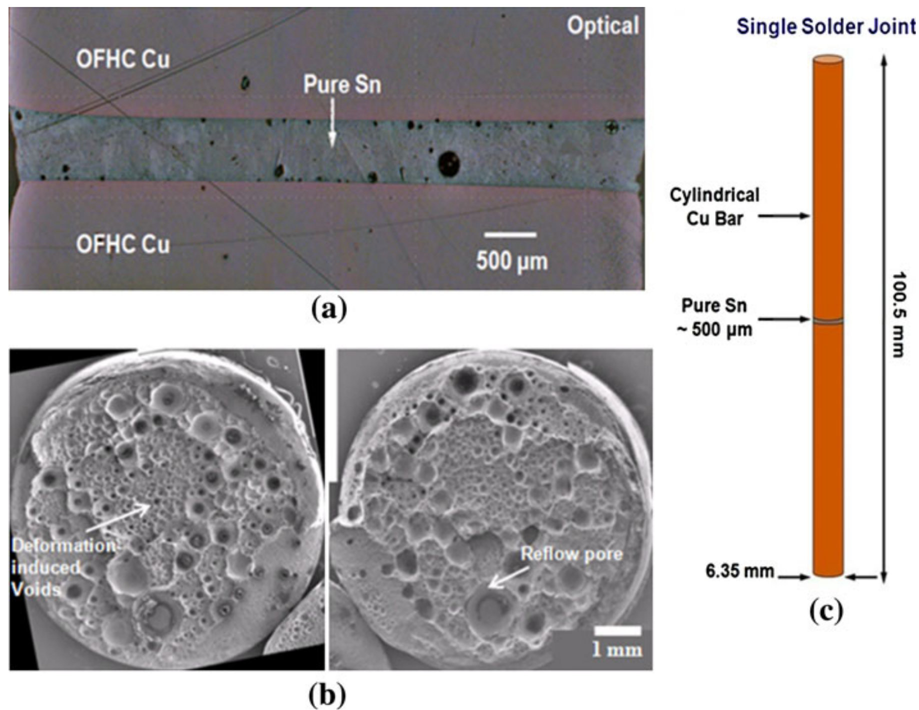

Fig. 1. Solder joint with microvoids before and after fracture. (a) Optical image of the side view of the joint. (b) Scanning electron microscopy image of the crack surface. (c) The overall geometry of the single solder joint with copper bar.

where σ_y is the yield stress of the matrix material. Tervgaard[17] suggests that q_1 is dependent on the strain-hardening behavior of the metal; for example, $q_1 = 1.25$ for $n = 20$ and $q_1 = 1.8$ for $n = 5$, where n is the strain-hardening exponent. It is also suggested that $q_2 = 1.0$ and $q_3 = q_1^2$. On setting the void volume fraction $f = 0$, the GTN collapses to the classical J_2 theory, which uses the von Mises stress as the yield condition. Figure 2 shows representative yield surfaces expressed as the relationship between normalized von Mises effective stress and hydrostatic stress for $q_1 = 1.8$ (for $n = 5$), $q_2 = 1.0$, and $q_3 = 3.24$. One can clearly see that the yield condition depends on both the von Mises stress and hydrostatic stress, and with increase of the void volume fraction, f, the material tends to yield at lower values of von Mises stress and hydrostatic stress.

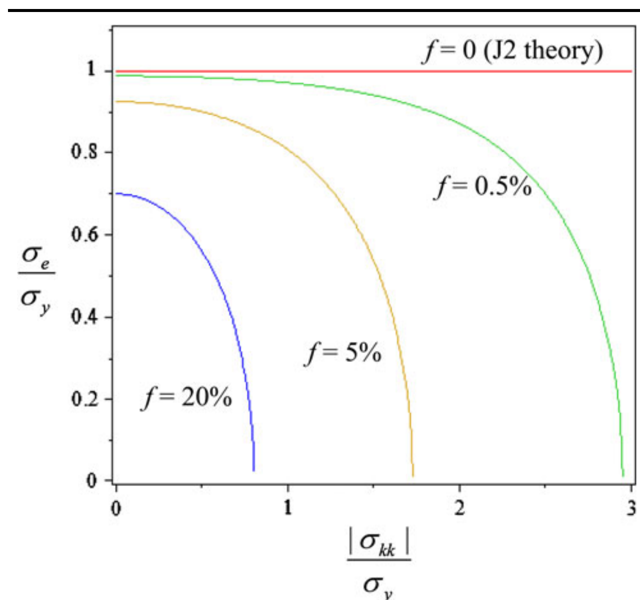

Fig. 2. Schematic of the yield surface of the GTN model; both von Mises stress and hydrostatic stress affect the yield criterion.

Figure 1 clearly shows that the voids are randomly distributed in the solder. Thus, it is necessary to be able to characterize the random nature of the initial void distribution. These initial voids may be induced due to reflow, for example. Because of the state variable, i.e., the void volume fraction f, introduced in the GTN model, the randomness of the voids can be implemented by assigning a randomly distributed initial void volume fraction, f, to each element. The randomly assigned initial void volume fraction f can have different distributions, e.g., Gaussian or rectangular distributions. Figure 3 shows an example random initial void distribution in a rectangular geometry. The two cases shown here have different initial void distributions. The average initial void volume fraction f is 0.5% for both random sets, and the range of random initial f of each element is from 0.01% to 1%, with a uniform distribution. This method was been implemented in the finite-element package ABAQUS.[13] The details of the porous plasticity with random initial void distribution can be found elsewhere.[13]

The finite-element analysis was conducted by using a commercial finite-element package ABAQUS (Providence, RI). The solder joint model consists of a Sn-rich solder alloy (i.e., water-quenched SAC), IMC layers of Cu_6Sn_5, and copper bars, as shown in Fig. 4. We assume perfect bonding between the IMC and solder, as well as IMC and copper. We have shown that these interfaces are quite strong, by atomistic-based simulations.[18] In fact, deformation by void growth in the Sn-rich alloy or cracking in the IMC layer will likely take place at much lower stresses compared with the interfacial

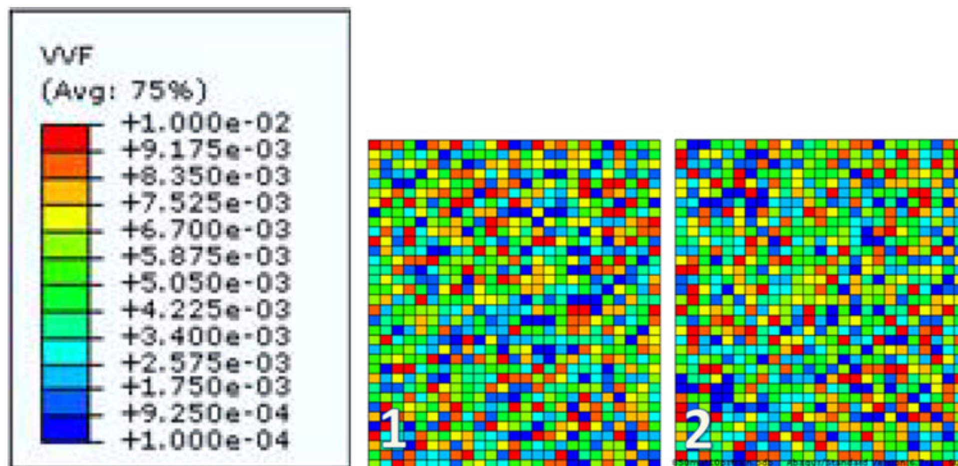

Fig. 3. Two random sets of initial void volume fraction for a rectangular geometry.

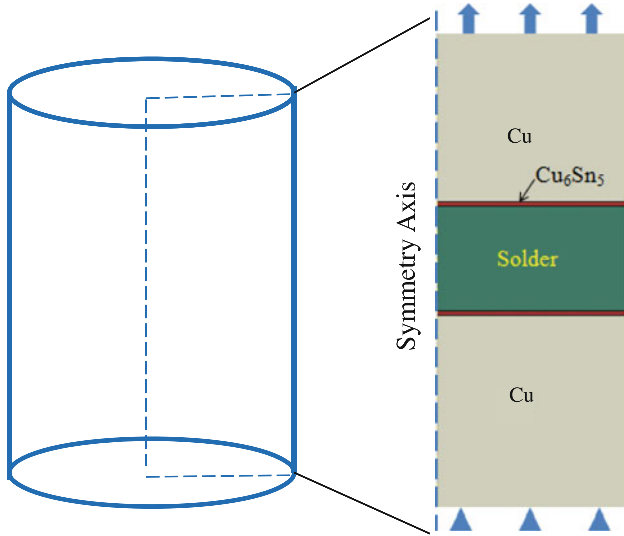

Fig. 4. Axisymmetric finite-element model of a solder joint with IMC.

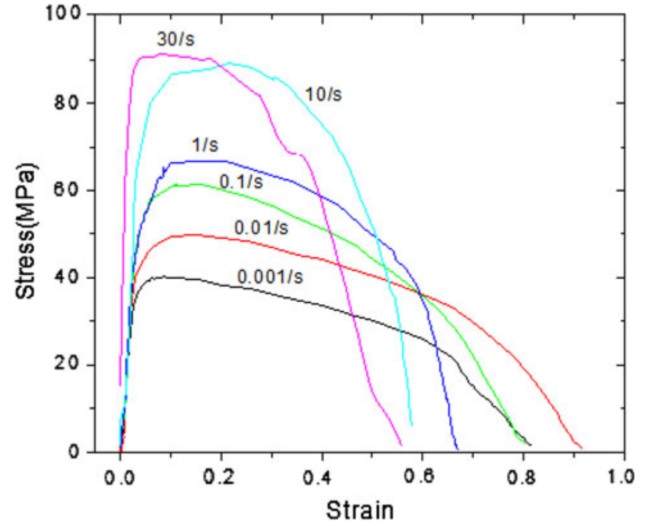

Fig. 5. Stress–strain curves of water-quenched SAC under different applied strain rates.

strength. The bottom of the model is fixed, and the top is subjected to a uniaxial tensile force. The axisymmetric boundary condition is applied at the symmetry axes. The solder is 0.5 mm in thickness and 6.35 mm in diameter, which are similar values to the experiments we conducted. The IMC thickness varies from a few to hundreds of micrometers.

The Cu_6Sn_5 IMC is modeled as a brittle material with Young's modulus of 112 GPa, Poisson's ratio of 0.3, density of 8.3 g/cm^3, yield strain of 1.2%, fracture stress of around 1350 MPa, and failure strain of 1.37%. These values were obtained experimentally from micropillar compression tests on in situ formed Cu_6Sn_5 in the joint.[19] The water-quenched SAC solder is modeled as a porous plastic material, with Young's modulus of 51 GPa, Poisson's ratio of 0.3, and density of 7.37 g/cm^3. The initial void volume fraction f for the solder is 0.5%, randomly distributed. Fracture results from void nucleation, growth, and coalesce. The void volume fraction at failure is set to 50% as an empirical value. The strain-rate dependence behavior of the solder was obtained by tensile tests on dog-bone specimens. The strain rate-sensitive behavior, ranging from strain rates of 0.001/s to 30/s, was used as the constitutive stress–strain behavior in the models, as shown in Fig. 5. The experimental data show, as expected, that a higher strain rate results in higher ultimate tensile strength (UTS), higher work-hardening rate, and lower ductility. With increasing strain rate, the solder has less time to relax and the local stresses becoming increasingly triaxial in nature. The randomness of the initial voids are considered and modeled by following the method discussed in "Finite-Element Modeling Approach" section. Because copper is much stiffer than the solder, the plastic deformation in copper is negligible and copper is thus modeled as an elastic material with Young's modulus of E = 116.5 GPa, Poisson's ratio of ν = 0.34, and density of 8.9 g/cm^3. Perfect bonding between the IMC and solder, as well as between IMC and copper are assumed. However, the elements next to the interface can fracture. Thus, fracture along the interface can be observed.

Simulations were conducted with ABAQUS/Explicit. Tensile velocity (displacement rate) along the axial direction was applied to maintain a nominal strain rate. The relation between velocity and strain rate is

$$\dot{\varepsilon} = \frac{\varepsilon}{t} = \frac{\Delta L}{t \cdot L} = \frac{v}{L}. \quad (2)$$

Axisymmetric elements were used in this study, namely CAX4R (four-node axisymmetric element with reduced integration) and CAX3 (three-node axisymmetric element). Mesh refinement was applied, and the details of the crack path and crack tips could be clearly illustrated. The solder region had about 10,000 elements, and the IMC region 2000 to 5000 elements depending on its thickness.

RESULTS AND DISCUSSION

In this section, we describe the results of our simulations. As mentioned above, the fracture mechanism is likely a function of the applied strain rate and the IMC thickness.[9] Therefore, the strain rate and IMC thickness effects are investigated in the following analysis.

In our initial simulations, we assumed that Cu_6Sn_5 is a homogeneous brittle material with uniform strength. In these simulations, the cracks occur only in the solder region, regardless of the strain rate or IMC thickness. Clearly, the IMC

needs to be modeled as a material with defects. It is well known that brittle materials, particularly ceramics, exhibit a volume dependence of strength. Larger volumes provide a greater chance of a strength-limiting flaw being present. Al_2O_3, for example, has much higher strength in fiber form than it does in bulk form.[20] Furthermore, tensile strengths of brittle materials are always higher than that in compression, because the flaws are closed in compression.

The fracture stress of Cu_6Sn_5 used in our simulations was computed by micropillar compression of single-crystal nodules. The pillars had diameter of about 1 μm and height of 2 μm. We expect that the behavior of the bulk IMC layer will have lower strength than the values obtained by pillar compression, because of the larger volumes and tensile stresses involved. Crystallography will likely not play much of a role in the strength variability as most nodules grow along the c-axis.[21]

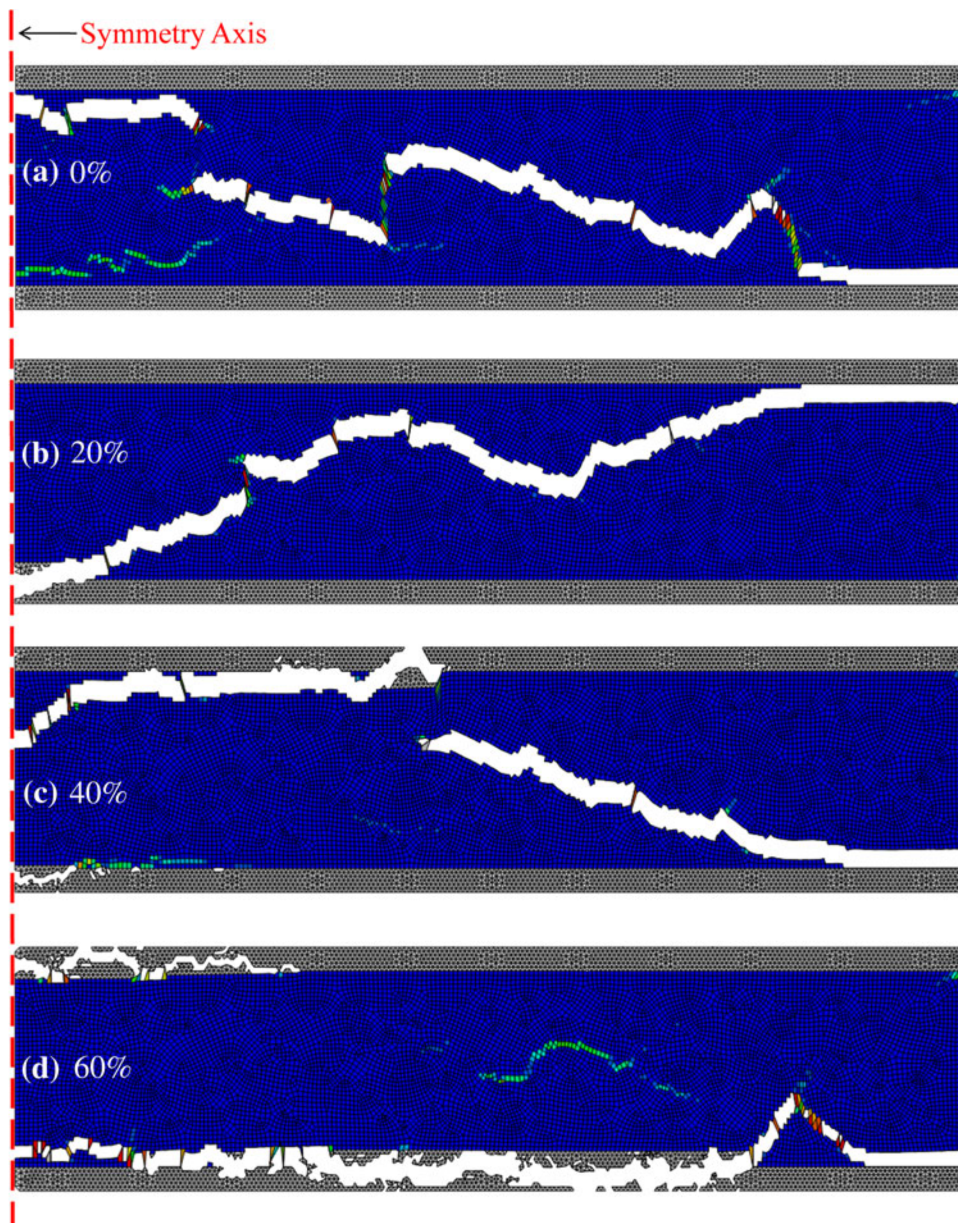

Fig. 6. Effect of randomly distributed "flawed" region of the inhomogeneous IMC. (a) No crack in homogeneous IMC region. (b) 20%, (c) 40%, (d) 60%. Large number of defective IMC elements results in more cracks in IMC region.

To introduce the strength variability within the IMC layer, due to microscopic flaws and defects, we used a method similar to that for the GTN model in "Finite Element Modeling Approach" section. The finite elements for Cu_6Sn_5 were randomly categorized into a number of groups, and each group had its individual fracture stress and failure strain, which were lower than obtained from the single-crystal microcompression test. These groups were randomly assigned so that the flawed elements were not all clustered together. In our finite-element analysis, around 20% to 60% of the total number of Cu_6Sn_5 elements were assigned lower fracture stress, which we term IMC "flawed" elements. Empirically, a range of fracture stress from 300 MPa to 600 MPa was used for the "flawed" elements.

To study the effect of defects in the IMC, four simulations with different fractions of "flawed" IMC elements, ranging from 0% to 60%, were conducted. The mesh consisted of 12,000 solder elements and 5000 IMC elements, the interface morphology was planar, the IMC thickness was kept constant at 80 μm, the strain rate was 30/s, and the initial void volume fraction f of the solder was f = 0.5%.

Figure 6 shows the contour of the void volume fraction of the solder joint (copper is not pictured). The solder region is blue, the IMC is gray, and the fractured region is white. Figure 6a shows the simulated fracture in Cu_6Sn_5 with no defects. All the cracks are in the solder region. Figure 6b–d shows fractured IMC layers with "flawed" element fraction of 20%, 40%, and 60%, respectively. These results show that, as the fraction of the defective IMC elements increases, the cracks tend to initiate within the IMC region.

There is experimental evidence that the IMC thickness affects the fracture behavior of solder joints.[14] We now present results on simulations showing the effect of IMC thickness, while keeping the microstructure and applied strain rate constant. The fraction of "flawed" IMC elements was fixed at 40% and the initial void volume fraction f for the solder was 0.5%, randomly distributed. The applied strain rate was 10/s. Three thicknesses of the IMC layer, 40 μm, 80 μm, and 120 μm, were studied.

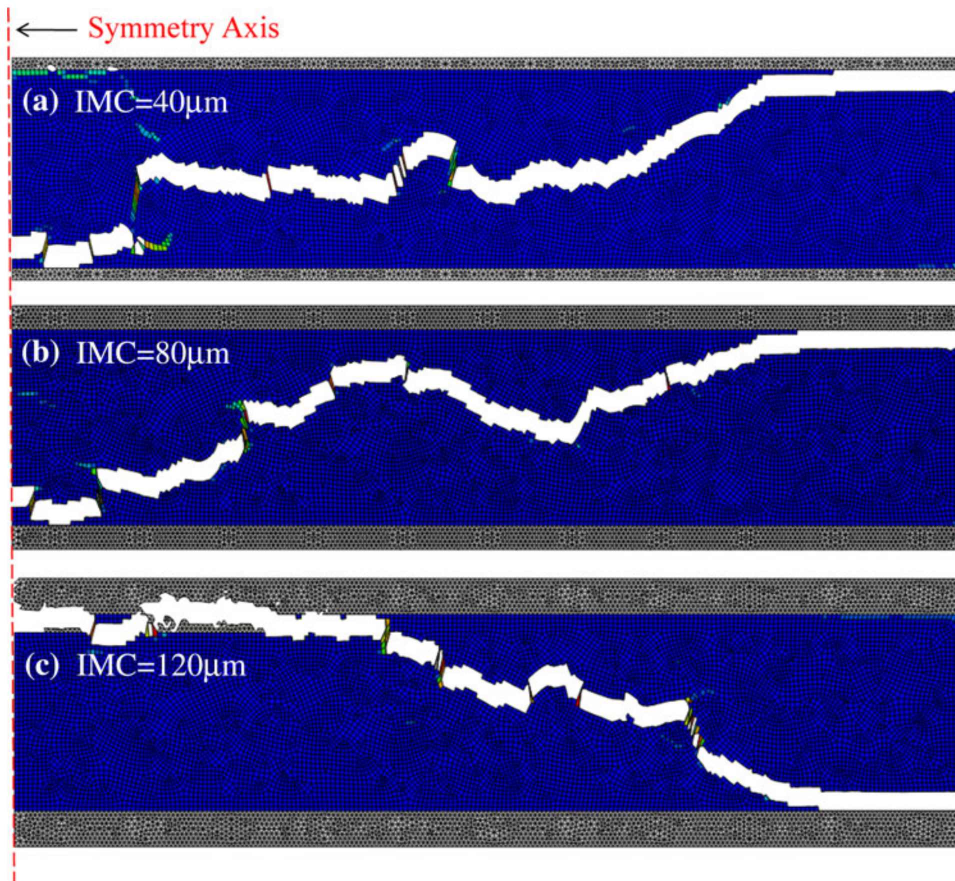

Fig. 7. IMC thickness effect of planar IMC under 10/s strain rate and 40% defected region for thickness of (a) 40 μm, (b) 80 μm, and (c) 120 μm. Thicker IMC induces more cracks in IMC region.

Figure 7 shows the results of the IMC thickness effect. The solder is shown in blue, IMC is gray, and the fractured region is white. In Fig. 7a, b, the IMC layer is relatively thin, and the cracks are mostly confined to the solder region. When the IMC thickness increases to 120 μm, as shown in Fig. 7c, fracture occurs in the IMC region. When the IMC layer is relatively thin, it provides sufficient bonding between the solder and copper.[22] When the IMC layer is thicker, IMC serves as a crack initiation site, leading to poor toughness of the joint, because of its brittle nature.[23–25]

The strain rate also greatly affects the fracture mechanisms in Pb-free solder joints.[9] Here we present the effects of strain rate. The IMC thickness was fixed at 120 μm, and the applied strain rate was varied from quasistatic (0.01/s) to dynamic (30/s). Other conditions and parameters were unchanged, specifically, the initial void volume fraction for the solder, f, of 0.5% and the fraction of flawed IMC elements of 40%. Figure 8a–d shows the crack patterns in the SAC solder joints at various strain rates. At lower strain rates (e.g., 0.01/s and 1/s for Fig. 8a, b), the cracks are in the solder region and the fracture is, thus, solder controlled. As the strain rate increases (e.g., $\dot{\varepsilon} = 10/s$ and $\dot{\varepsilon} = 30/s$ for Fig. 8c, d), fracture occurs in both the solder and IMC regions. At strain rate of 30/s (Fig. 8d), the

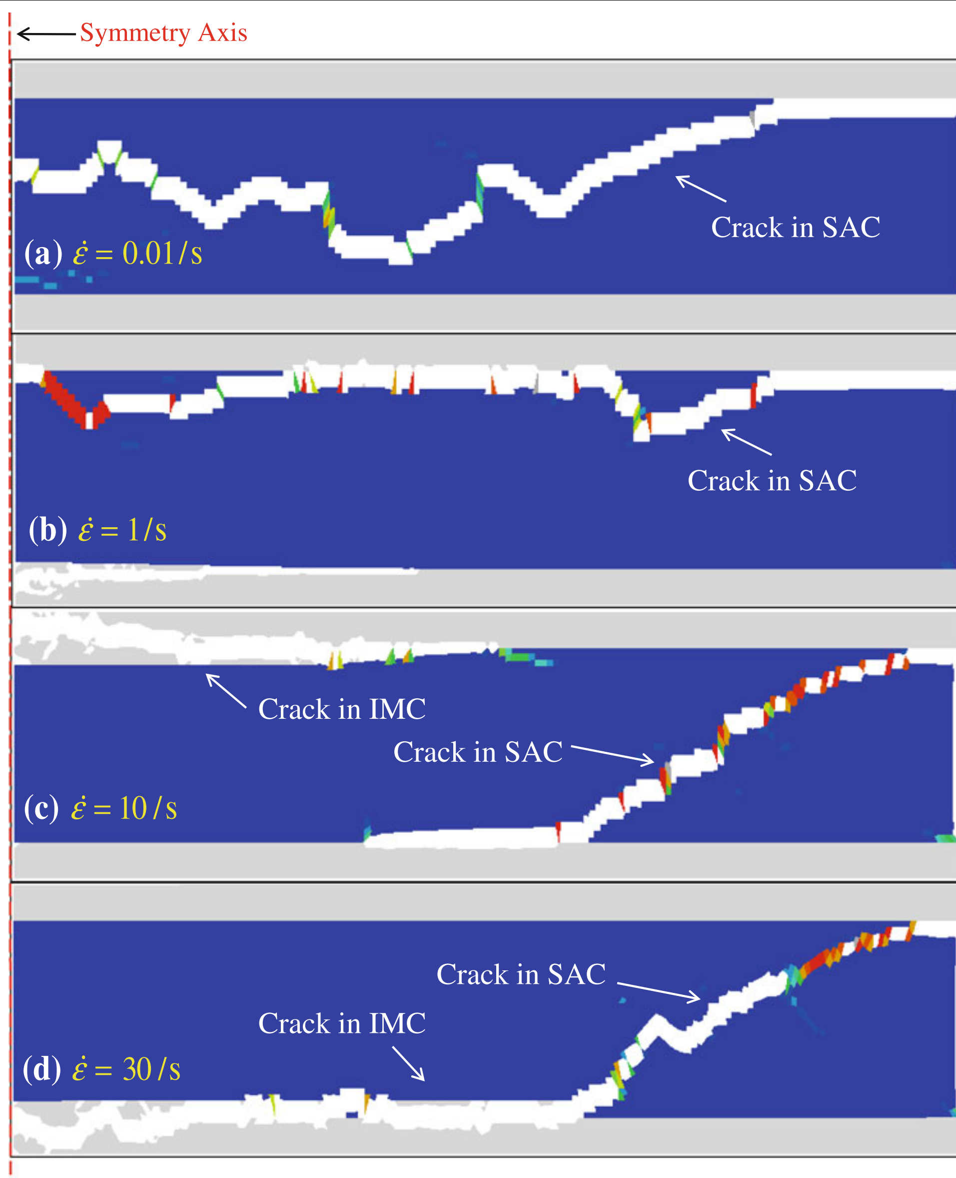

Fig. 8. Strain rate effect of planar IMC with 120-μm-thick IMC and 40% defective region for strain rates of (a) 0.01/s, (b) 1/s, (c) 10/s, and (d) 30/s. Higher applied strain rate induces more cracks in IMC region.

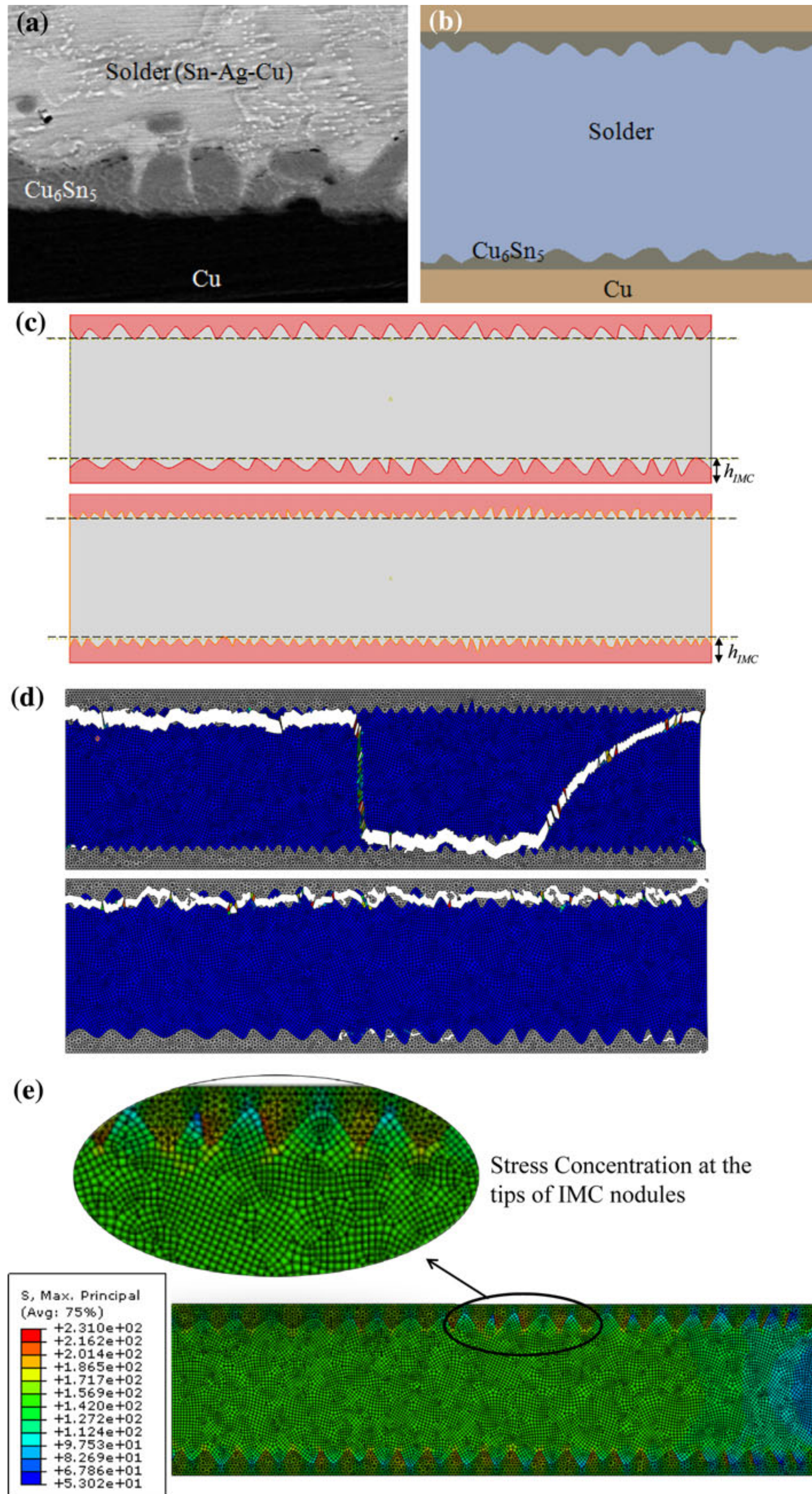

Fig. 9. (a) Experimental image of a solder joint showing a nodule-shaped IMC. (b) Finite-element analysis model with a wavy-shape IMC/solder interface. (c) Two solder joints with the same IMC thickness; one has coarse nodules, and the other has smaller and finer nodules. (d) Fracture pattern of these two solder joints. (e) Maximum principal stress distribution (concentrations at the nodules).

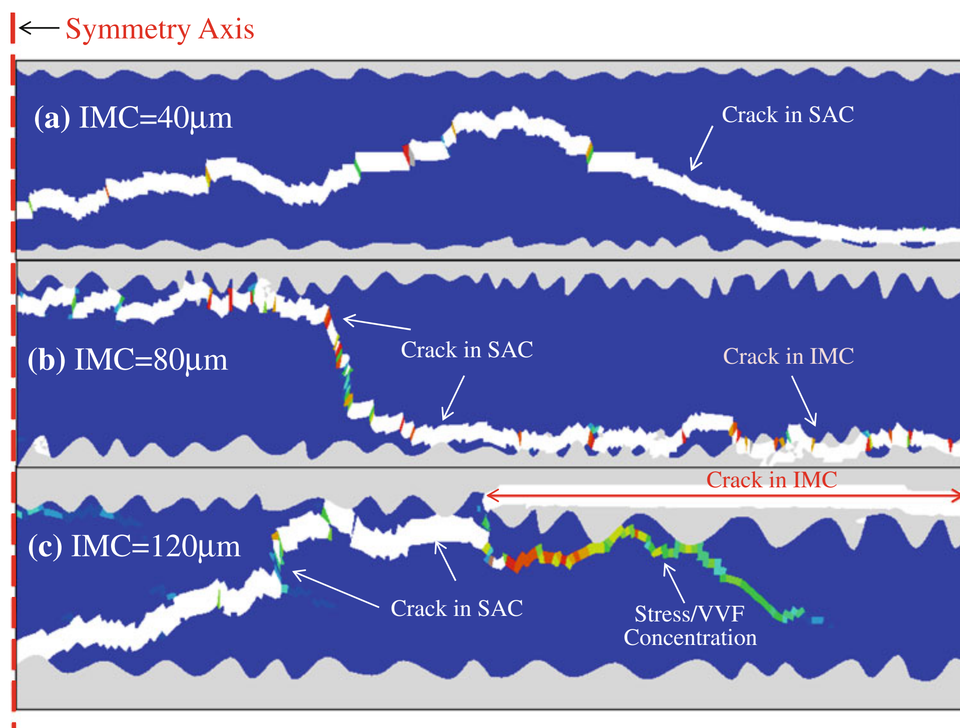

Fig. 10. Thickness effect of nodule IMC. Contour of void volume fraction and crack path of three cases with IMC thickness of (a) 40 μm, (b) 80 μm, and (c) 120 μm. Thicker IMC induces more cracks in IMC region.

length of fractured IMC is even more than half of the total crack length, which is certainly IMC-controlled fracture.

The dominant fracture mechanism, i.e., solder-controlled or IMC-controlled fracture, is a result of the competition between stress relaxation in the solder and brittle fracture and catastrophic crack propagation within the IMC layer. Cu_6Sn_5 is certainly much stiffer than water-quenched SAC, and has a much lower strain to failure. At quasistatic or relatively low strain rates, the solder yields, and ductile fracture takes place before cracking can nucleate within the Cu_6Sn_5 layer. At higher strain rates, however, the solder cannot relax and a state of high stress triaxiality builds up within the solder, so the IMC becomes more important and brittle fracture can initiate in the IMC layer, particularly at microscopic flaws.

In experiments, the morphology of the IMC is not planar, as shown in Figs. 7 and 8, but rather nodular, as shown in Fig. 9a. The formation of the nodules is due to the diffusion and reaction between Sn-rich liquid (during melting) and copper substrate, as well as pinning of Cu_6Sn_5 during growth.[26,27] To mimic the nodule shape of IMC, a wavy interface between solder and IMC was modeled, as shown in Fig. 9b. The thickness of the nodule IMC layer is defined as the distance from the top of the nodule to the IMC/Cu interface. It is assumed that all the nodules have similar height, and extreme cases, such as where one or two nodules are much thicker than others, are not considered. Figure 9c illustrates two solder joints (only solder and IMC parts are shown) with the same IMC thickness but different morphology. The top one has coarse nodules, and the bottom one has smaller and finer nodules.

We first describe the effect of nodule morphology, i.e., coarse versus fine nodules. The nodule thickness is 120 μm; the percentage of the defective IMC is 40%, and the initial random distributed void volume fraction f in solder is 0.5%. The strain rate is 10/s. The finite-element analysis results are shown in Fig. 9d, which indicates that coarse nodules result in more IMC-controlled fractures. The possible mechanism for this is that larger nodules have higher stress concentration at the wavy interface, while a finer nodule induces less stress concentration, and the planar-shape IMC has no stress concentration at the interface. Figure 9e shows the maximum principal stress for the coarse nodule case, where stress concentration exists for the coarse nodules. The IMC nodules increase the possibility of IMC-controlled fracture.

Secondly, we studied the effect of the thickness of the nodular IMC on the solder joint fracture. All the simulation conditions were the same as those used in Fig. 9, except that the thicknesses of the nodules were 40 μm, 80 μm, and 120 μm. Here, we must point out that the nodule shapes for different nodule

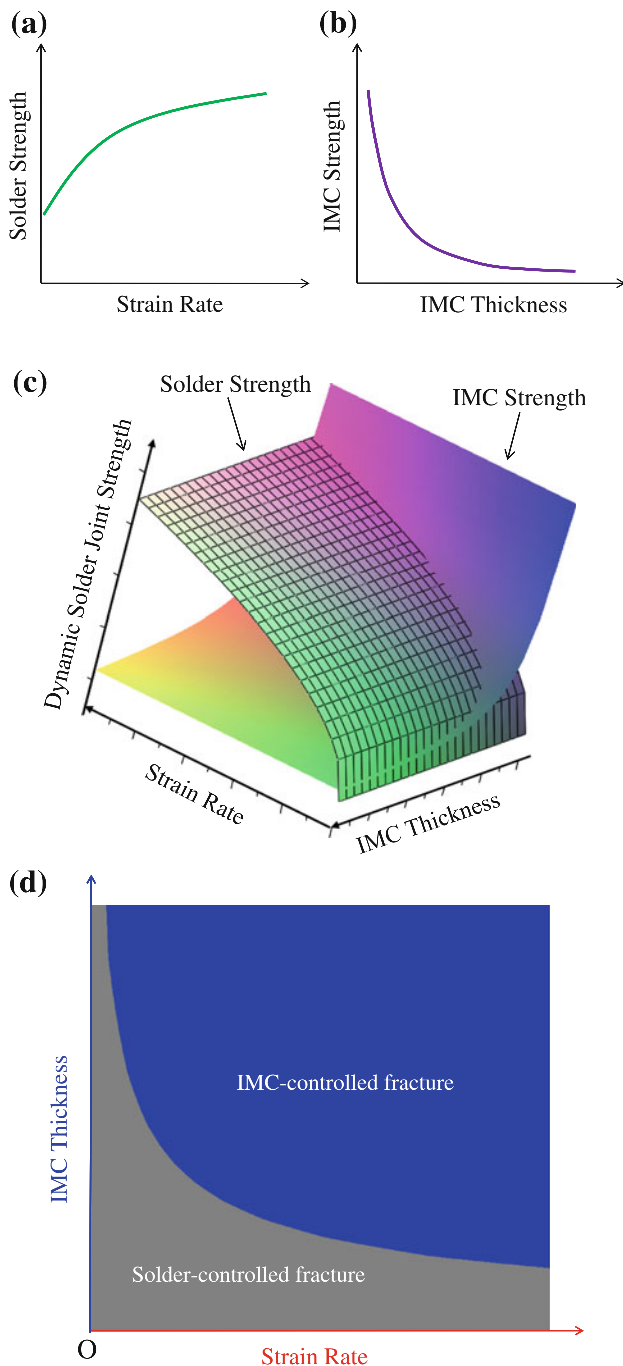

Fig. 11. (a) Fracture strength of solder increases with strain rate. (b) Fracture strength of IMC decreases with IMC thickness. (c) 3-D relation coupling the IMC thickness effect and applied strain rate effect together. (d) Solder-controlled and IMC-controlled fracture as a function of both strain rate and IMC thickness.

thickness are not self-similar, despite the fact that they are all coarse nodules. Figure 10 shows the finite-element results. First, the trend is the same as that for the planar IMC, i.e., thicker IMC layer induces more cracks in the IMC region. Second, more IMC-controlled fracture is present in the nodular IMC than that in planar IMC under the same conditions.

CONCLUSIONS

We conducted finite-element analysis to study solder joint fracture under dynamic loading conditions. The solder is modeled as a porous plastic material and the IMC as an elastic material. The fracture of the solder is governed by void nucleation, and the IMC is assumed to fail by brittle failure. The randomness of the void volume fraction in the solder and the flaws in IMC are considered and implemented in the finite-element package ABAQUS. The finite-element results show that the fracture mechanisms of the solder joints depend on the strain rate and IMC thickness. Higher strain rates and larger IMC thickness favor IMC-controlled fracture, which is brittle in nature. Lower strain rate and smaller IMC thickness lead to solder-controlled fracture, which is governed by void growth and nucleation. This observation agrees very well with experiments.[9]

The fundamental mechanism is competition between the fracture strength of the solder and the IMC. At lower strain rates, the solder deforms plastically and deformation is solder controlled. At higher strain rates, the stress state is more triaxial. As the thickness of the IMC increases, flaws in the IMC with lower fracture strength become more likely, so that IMC-controlled fracture may occur. This effect is more prevalent at higher strain rates, as well. Therefore, the fracture of the solder joint depends on both strain rate and IMC thickness.

To qualitatively illustrate the mechanism of solder joint fracture, a “mechanism diagram” of solder joint fracture is suggested in Fig. 11. The fracture strength of solder increases with strain rate (Fig. 11a), while that of IMC decreases with IMC thickness (Fig. 11b). The intersection between the fracture strength of solder and of IMC forms the critical condition for solder joint fracture (Fig. 11c). The projection of the intersection line is shown in the IMC thickness/strain rate space (Fig. 11d). Clearly, the line separates the solder-controlled fracture (ductile) and IMC-controlled fracture (brittle).

We have a few remarks regarding the findings of this paper. Firstly, there exists some reported work on IMC-controlled or solder-controlled fracture as a function of IMC thickness and applied strain rate. The present study is more comprehensive and systematic in terms of modeling and simulation, rather than providing intuitive explanation. Secondly, the effect of nodular IMC should be considered in conjunction with the effect of IMC thickness, because the waviness and thickness change together with thermal aging, i.e., the waviness decreases and the thickness increases with thermal aging. During long-term thermal aging, the IMC phase becomes inhomogeneous as Cu_3Sn is formed.[28,29] This effect

was not considered in the current study, but can be incorporated using this approach. Thirdly, the present study focuses on mechanical shock behavior where the deformation is temperature independent, which is different from the deformation under thermal cycling conditions where the behavior is strongly temperature dependent.[30]

ACKNOWLEDGEMENTS

The authors are grateful for financial support for this work from the National Science Foundation, Division of Materials Research—Metals Division, DMR-0805144 (Drs. A. Ardell, B. Macdonald, and H. Chopra, Program Managers). We also appreciate the Fulton High Performance Computing at Arizona State University for support of our simulations.

REFERENCES

1. K. Zeng and K.N. Tu, *Mater. Sci. Eng. Rep.* 38, 55 (2002).
2. R.S. Sidhu and N. Chawla, *Metall. Mater. Trans. A* 39A, 340 (2008).
3. P.L. Hacke, A.F. Sprecher, and H. Conrad, *J. Electron. Mater.* 26, 774 (1997).
4. R.S. Sidhu, X. Deng, and N. Chawla, *Metall. Mater. Trans. A* 39A, 349 (2008).
5. D. Reiff and E. Bradley, *Electronic Components and Technology Conference* (2005), p. 1519.
6. M. Date, T. Shoji, M. Fujiyoshi, K. Sato, and K.N. Tu, *Electronic Components and Technology Conference* (IEEE, 2004), p. 668.
7. R. Pandher and M. Boureghda, *45th Annual International Reliability Physics Symposium* (2007), p. 107.
8. K. Newman, *Proc. 55th Electronic Components & Technology Conference* (2005), p. 1194.
9. N. Chawla, *Int. Mater. Rev.* 54, 368 (2009).
10. D. Suh, D.W. Kim, P.L. Liu, H. Kim, J.A. Weninger, C.M. Kumar, A. Prasad, B.W. Grimsley, and H.B. Tejada, *Mater. Sci. Eng. A* 460, 595 (2007).
11. Y.L. Liu, S. Gale, and R.W. Johnson, *IEEE Trans. Electron. Packag. Manuf.* 30, 63 (2007).
12. T.T. Mattila, P. Marjamaki, and J.K. Kivilahti, *IEEE Trans. Compon. Packag. Technol.* 29, 787 (2006).
13. H. Fei, K. Yazzie, N. Chawla, and H. Jiang, *J. Electron. Mater.* 41, 177 (2012).
14. X. Deng, R.S. Sidhu, P. Johnson, and N. Chawla, *Metall. Mater. Trans. A* 36A, 55 (2005).
15. F. Ochoa, J.J. Williams, and N. Chawla, *J. Miner. Met. Mater. Soc.* 55, 56 (2003).
16. A.L. Gurson, *J. Eng. Mater. T* 99, 2 (1977).
17. V. Tvergaard, *Int. J. Fract.* 17, 389 (1981).
18. H.Y. Fei, K. Yazzie, J. Williams, N. Chawla, and H.Q. Jiang, *J. Comput. Theor. Nanosci.* 8, 873 (2011).
19. L. Jiang and N. Chawla, *Scr. Mater.* 63, 480 (2010).
20. N. Chawla, M. Kerr, and K.K. Chawla, *J. Am. Ceram. Soc.* 88, 101 (2005).
21. L. Jiang, H. Jiang, and N. Chawla, unpublished.
22. P. Protsenko, A. Terlain, V. Traskine, and N. Eustathopoulos, *Scr. Mater.* 45, 1439 (2001).
23. D.R. Frear, *J. Miner. Met. Mater. Soc.* 48, 49 (1996).
24. D.R. Frear and P.T. Vianco, *Metall. Mater. Trans. A* 25, 1509 (1994).
25. R.E. Pratt, E.I. Stromswold, and D.J. Quesnel, *J. Electron. Mater.* 23, 375 (1994).
26. Z. Mei, A.J. Sunwoo, and J.W. Morris, *Metall. Trans. A* 23, 857 (1992).
27. S. Choi, T.R. Bieler, J.P. Lucas, and K.N. Subramanian, *J. Electron. Mater.* 28, 1209 (1999).
28. L. Xu and J.H.L. Pang, *Proceedings—IEEE Electronic Components and Technology Conference* (2006), p. 275.
29. J. Varghese, B. Song, M. Azarian, A. Dasgupta, and M. Pecht, *Proceedings of the ASME International Mechanical Engineering Conference and Exposition* (2005), p. 82428.
30. R.S. Sidhu and N. Chawla, *Metall. Mater. Trans.* 39A, 799 (2008).